Organic Electronics 107 (2022) 106560

Contents lists available at ScienceDirect

Organic Electronics

journal homepage: www.elsevier.com/locate/orgel

Layer-by-layer solution-process enables higher crystallinity and desirable phase separation in non-fullerene organic solar cells

Xin Liang [a,b], Shuai Zhang [b], Yuanwei Wu [b], Jiuxing Wang [a,**], Chunpeng Yang [b], Aziz Saparbaev [b,d], Shuguang Wen [b,c,***], Xichang Bao [b,c,*]

[a] Institute of Hybrid Materials, National Center of International Joint Research for Hybrid Materials Technology, National Base of International Science & Technology Cooperation, College of Materials Science and Engineering, Qingdao University, Qingdao, 266071, China
[b] Qingdao Institute of Bioenergy and Bioprocess Technology, Chinese Academy of Sciences, Qingdao, 266101, China
[c] Functional Laboratory of Solar Energy, Shandong Energy Institute, Qingdao, 266101, China
[d] Institute of Ion-Plasma and Laser Technologies of Uzbekistan Academy of Sciences, National University of Uzbekistan Named After Mirzo Ulugbek, Tashkent, 100125, Uzbekistan

A B S T R A C T

Device engineering is one of the effective ways to improve the photovoltaic performance of organic solar cells. In particular, the performance of some materials may not be poor, and morphology control is more important to make efficient charge generation and transport, and inhibit exciton recombination. In this work, LBL and conventional OSCs based on PBB-TSD donor and Y6 acceptor were prepared. Compared with conventional OSCs. The LBL process improves the dissociation of excitons, inhibits charge recombination and promotes charge transfer in the active layer. Hence, a power conversion efficiency (PCE) of 11.84% with a short-circuit current density (J_{SC}) of 23.52 mA cm^{-2} is obtained in the LBL-type OSCs, which are both higher than that of the BHJ-type OSC (PCE = 10.77%, J_{SC} = 21.19 mA cm^{-2}). These results indicate that LBL process would be a more efficient device structure than that of BHJ with PBB-TSD:Y6 as the active layer.

1. Introduction

In recent years, organic solar cells (OSCs) have attracted a lot of attention for their advantages such as light-weight, flexibility, low-cost, solution printing [1–5]. The photovoltaic performance of solution-processed OSCs is primarily determined by the active materials and film morphology [6,7]. In the past decades, solution-processed OSCs have developed rapidly due to the continuous exploration of novel donors and acceptors with improved light harvesting ability, suitable energy levels distribution, and good compatibility [8–14]. The power conversion efficiencies (PCEs) of single layer devices based on well-matched conjugated donors and non-fullerene acceptors have exceeded 18% [15–18]. In addition to the achievements in materials, the optimization of device structures and innovation of device processes are also very important for the rapid development of OSCs [19–23].

Bulk heterojunction structures (BHJs) have attracted much attention due to the bicontinuous interpenetrating networks with sufficient donor/acceptor interfaces for effective excitons dissociation [24–26]. Thus, BHJs have become the main method for preparing the active layers of OSCs [15,16,27,28]. It is well known that good miscibility, complementary absorption spectra, and matching energy levels between donor and acceptor of the devices are the premise to achieve high efficiency. Some donor polymers have strong self-aggregation behavior, and the BHJ process would restrict the formation of nanoscale interpenetrating networks between donor and acceptor materials, which could limit the corresponding OSCs from achieving good performance. Furthermore, some materials have different solubility in different solvents, and it is of great significance to study new device processing. The LBL process, which prepares thin films by sequentially depositing electron donor and acceptor layers, can offer the possibility to solve this problem [29–35]. In addition, the independent processing of donor and acceptor layers facilitates the control of molecular aggregation and crystallization to obtain a suitable film morphology [36,37]. Usually, there exhibits a similar p-i-n structure and vertical phase separation in LBL films, which facilitates improving charge transfer and reducing charge recombination, thus improving photovoltaic properties of OSCs [22,38–40].

In this work, we fabricated two kind devices based on polymer donor

Abbreviations: 1, Organic solar cells; 2, LBL process; 3, Crystallinity; 4, Phase separation.

* Corresponding author. Qingdao Institute of Bioenergy and Bioprocess Technology, Chinese Academy of Sciences, Qingdao, 266101, China.
** Corresponding author.
*** Corresponding author. Qingdao Institute of Bioenergy and Bioprocess Technology, Chinese Academy of Sciences, Qingdao, 266101, China.
E-mail addresses: jiuxingwang@qdu.edu.cn (J. Wang), wensg@qibebt.ac.cn (S. Wen), baoxc@qibebt.ac.cn (X. Bao).

https://doi.org/10.1016/j.orgel.2022.106560
Received 12 April 2022; Received in revised form 13 May 2022; Accepted 15 May 2022
Available online 23 May 2022

PBB-TSD and acceptor Y6, and both of the molecular structures are given in Fig. 1a. To distinguish the two devices, we label the LBL devices and the BHJ devices as PBB-TSD/Y6 and PBB-TSD:Y6, respectively. Despite the materials have complementary absorption and matched energy levels, the photovoltaic performance of BHJ device is still undesirable, which is attributed to the poor miscibility. OSCs fabricated by LBL method were investigated to achieve desirable morphology and vertical phase separation of the active layers. It is well established that the ratio, concentration, thickness and thermal annealing of the donor and acceptor materials would affect the vertical distribution of the donor and acceptor in the active layer. Benefiting from the LBL process, devices exhibit higher crystallinity, suitable vertical phase separation and balanced carrier mobilities. Ultimately, the LBL device achieves higher short-circuit current density (J_{SC}) of 23.52 mA cm^{-2} and power conversion efficiency (PCE) of 11.84%, with regard to the BHJ devices (J_{SC} = 21.19 mA cm^{-2}, PCE = 10.77%). These results indicate that LBL processing is a reliable approach to be investigated in some defined system in OSCs.

2. Results and discussion

The molecular structures, energy levels and absorption of PBB-TSD and Y6 are shown in Fig. 1. In PBB-TSD, the BDT nucleus with alkyl side chain was used as the electron donor unit and the BBT nucleus was used as the electron acceptor unit. The introduction of S weakens the donor conjugation effect and lower the HOMO level of PBB-TSD. This is critical for charge transfer in the vertical direction of the substrate, thus reducing charge recombination. PBB-TSD shows main face-to-face orientation and high crystallinity. PBB-TSD shows strong absorption in the range of 300–615 nm, and Y6 shows strong absorption in the range of 600–900 nm, which indicate a good complementary absorption between PBB-TSD and Y6. The LUMO energy levels of PBB-TSD and Y6 are −3.56 and −4.10 eV respectively, and the gap between them provides sufficient driving force for exciton dissociation. Thus, the related OPVs could have good current density both in terms of absorption and energy levels.

Two kind devices were fabricated with the conventional structure of ITO/poly(3,4-ethylene dioxythiophene): polystyrene-polystyrene sulfonate (PEDOT:PSS)/active layer/PDINO/Al, and the device structure diagram is shown in Fig. 2a. The UV–Vis absorption spectra of LBL and BHJ films based on PBB-TSD and Y6 are shown in Fig. 2b. As can be seen from the UV–Vis absorption spectra, the LBL and BHJ films show very similar hump-shaped profiles covering wide absorption wavelength range from 300 to 1000 nm. Both the LBL and BHJ films show two obvious peaks at around 540 nm and 585 nm in short wavelength region, indicating the strong aggregation behavior of PBB-TSD in both films. Compared to the BHJ film, the LBL film exhibits slightly red-shifted absorption peak, which demonstrates the enhanced molecular ordering of Y6 [34]. This facilitates charge transfer, which could have a positive impact on the boosting of current of the LBL device.

The current density-voltage (*J-V*) curves of the LBL and BHJ OSCs were measured under AM 1.5G illumination with 100 mW cm^{-2} light intensity, as shown in Fig. 2c. And the relevant parameters of these devices are summarized in Table 1. It can be seen that the LBL OSC exhibit higher photovoltaic performance with a PCE of 11.84% than that of the BHJ OSCs (10.77%). It can be seen that the LBL device shows a slightly lower open-circuit voltage (V_{OC}) of 0.85 V than that of BHJ device (0.87 V), which may be caused by the fine difference of the film

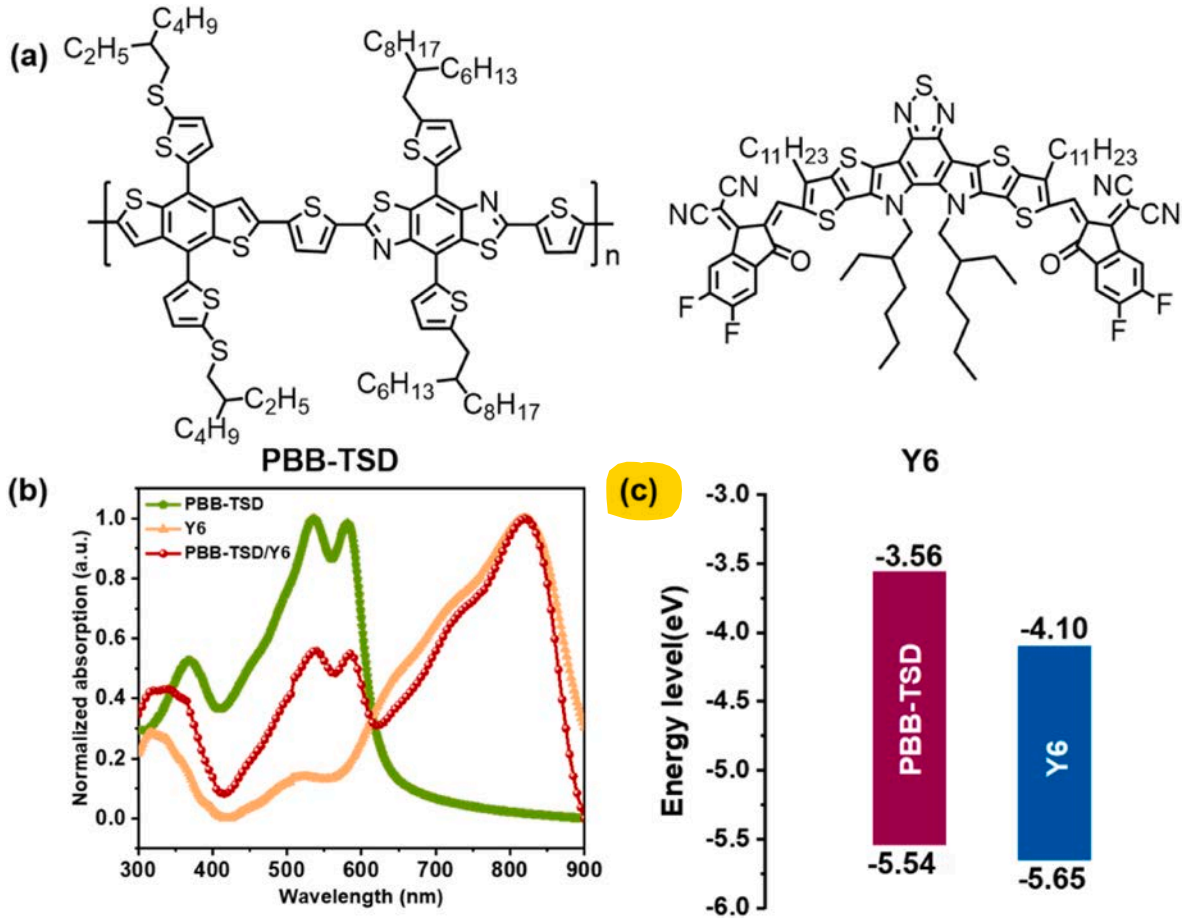

Fig. 1. (a) Molecular structures of PBB-TSD and Y6. (b) Normalized absorption spectra of PBB-TSD, Y6 and PBB-TSD/Y6 films. (c) Energy level diagrams of PBB-TSD and Y6.

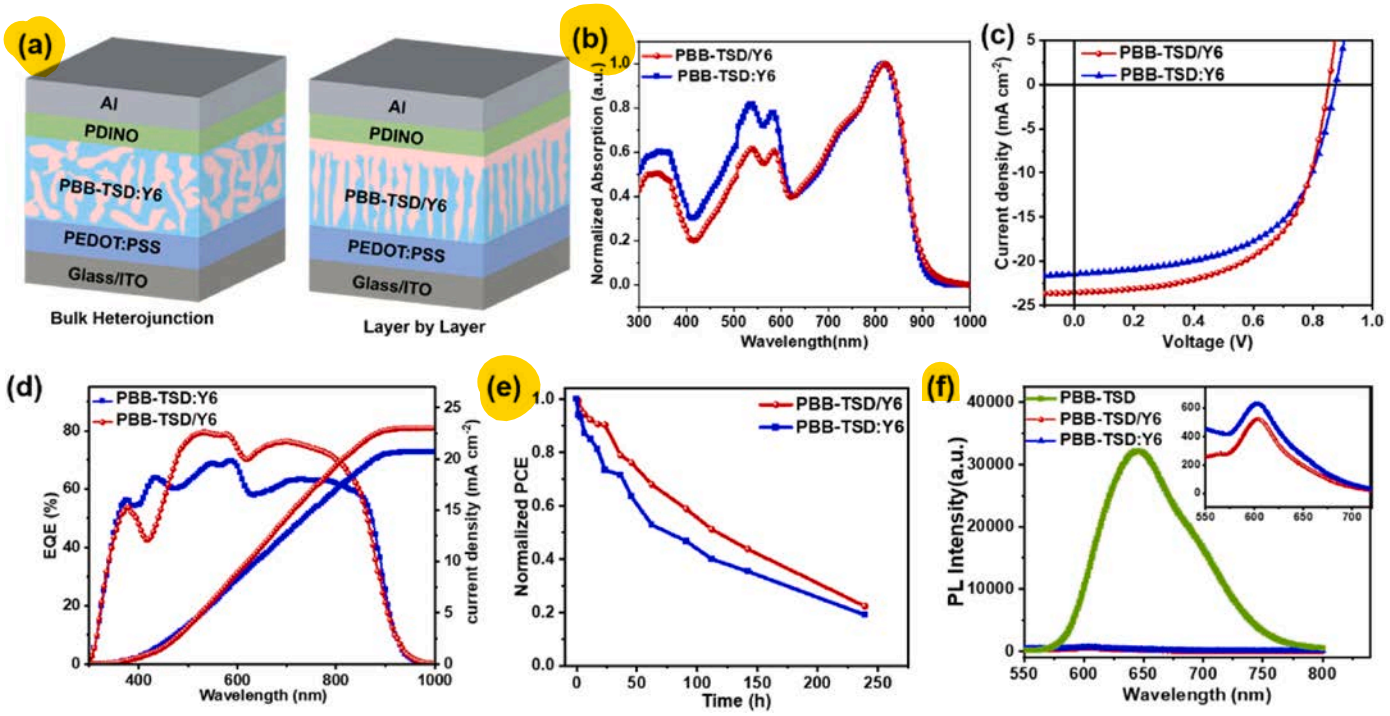

Fig. 2. Schematic diagram of device structure (a), absorption spectra (b), $J-V$ curves (c), EQE spectra (d) and stability (e) for BHJ and LBL OSCs. (f) PL quenching spectra of pristine PBB-TSD and LBL and BHJ films.

Table 1
Photovoltaic parameters of the two kind OSCs.

Device	V_{OC} (V)	J_{SC} (mA cm^{-2})	FF (%)	PCE (%)	R_S (Ω)[a]	R_{SH} (Ω)[a]
BHJ: PBB-TSD:Y6	0.87	21.19	58.05	10.77	6.45	445.54
LBL: PBB-TSD/Y6	0.85	23.52	59.06	11.84	5.02	615.14

[a] The values are obtained from the *J-V* curves.

quality. And there is no clear trends of changes so far [22,32,34,35]. However, the LBL devices exhibit improved short-circuit current density (J_{SC}) and fill factor (FF). The J_{SC} and FF of the BHJ OSC are 21.19 mA cm^{-2} and 58.05%, respectively, and the LBL OSC exhibits higher J_{SC} of 23.52 mA cm^{-2} and FF of 59.06%. In addition, the structure of LBL device can reduce the recombination at interface of electrode. The LBL devices show a series resistance (R_S) of 5.02 Ω, which is smaller than that of BHJ devices (6.45 Ω). Furthermore, BHJ device exhibits a shunt resistance (R_{SH}) of 445.54 Ω, while LBL devices exhibit a larger R_{SH} of 615.14 Ω, which means that LBL devices have less leakage current than that of BHJ devices. The larger R_{SH} and smaller R_S indicate that LBL devices have improved charge transport and less charge recombination, which is the reason for high FF of LBL devices.

External quantum efficiency (EQE) curves are tested to examine the spectral response and photocurrent generation in both LBL and BHJ devices, as shown in Fig. 2d. Both BHJ and LBL devices show wide photo response range from 300 to 900 nm, which is accordant with the absorption spectra of the blend films. Moreover, the LBL device exhibits a significantly higher curve than BHJ device in the range from 460 to 840 nm, which could account for the higher J_{SC} and PCE of LBL device. The J_{SC} values calculated from the EQE spectra of the BHJ and LBL devices are 20.67 and 22.99 mA cm^{-2} respectively, which are within 5% error of the J_{SC} values measured by the *J-V* curves, thus establishing the validity of the results. The slightly lower calculated J_{SC} values are mainly attributed to the EQE spectrum of the device tested in an air environment without any packaging. The absorption spectra of the active layer are different from the EQE spectra, which should be attributed to the interference effect between the incident light and the reflected light from the aluminum electrode [19,41]. The results further confirmed that LBL process can form vertical phase separation, which is convenient for charge transport and collection.

The stability of both BHJ and LBL OSCs in a nitrogen-filled glove box are tested [42]. Fig. 2e shows the normalized time evolution parameters of the PCE for both BHJ and LBL devices, the devices show similar decay tendencies, while the LBL OSCs exhibit better stability. After 240 h of placement, the PCE of LBL and BHJ OSCs decreased to 22.36% and 19.12%, respectively. This indicates that the LBL devices have better tolerance to time due to the optimized active layer and improved surface topography. Photoluminescence (PL) spectra of BHJ and LBL films were measured to elucidate the process of exciton utilization in the active layer, as shown in Fig. 2f. The samples were examined by exciting the PBB-TSD at 560 nm to detect the dissociation and charge transfer efficiency at the D/A interface. Both the LBL and BHJ films exhibit significant fluorescence quenching, indicating efficient electron transfer from the donor to the acceptor. Among them, the fluorescence quenching efficiency of the LBL films are higher than those of the BHJ films, indicating that the LBL films have higher exciton dissociation efficiency. In addition, we also investigate the dependence of J_{SC} and V_{OC} on light intensity (P_{light}) to reveal the charge transfer and recombination processes of the devices under the two fabrication processes. The relationship between J_{SC} and P_{light} can be described by $J_{SC} \propto (P_{light})^{\alpha}$ [43]. As shown in Fig. 3a, the α value for LBL-type OSC (0.886) is closer to 1, which is larger than that of α value for BHJ-type OSCs (0.878). The results show that LBL devices can more effectively suppress bimolecular recombination. The dependence of V_{OC} on P_{light} follows the equation $V_{OC} \propto (nkT/q)\ln(P_{light})$, where n is constant, K is Boltzmann's constant, T is Kelvin temperature, and q is elementary charge. The parameter n (mostly $1 < n < 2$) describes the trap-assisted charge carrier recombination in the device. If n is close to 2, it indicates that the recombination process in the device is dominated by monomolecular (trap-assisted) recombination [44]. If n is close to 1, it indicates weak bimolecular recombination in the device. The values of n for PBB-TSD/Y6 and PBB-TSD:Y6 based devices as shown in Fig. 3b are 1.065 and 1.199,

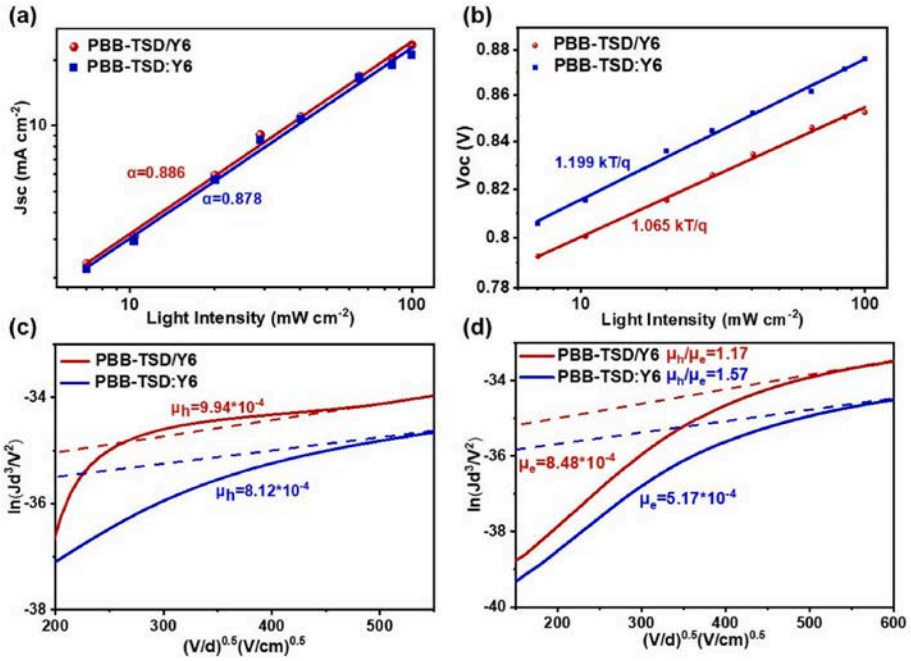

Fig. 3. Light intensity dependence of (a) J_{SC}, and (b) V_{OC} for LBL and BHJ OSC. SCLC fitting curves of LBL and BHJ (c) hole-only and (d) electron-only devices.

respectively. This indicates that PBB-TSD/Y6 devices have less trap-assisted recombination compared to the PBB-TSD:Y6 devices, which is advantageous for obtaining higher FF values.

In order to verify the effect of LBL process on charge transfer characteristics, the charge mobilities of LBL and BHJ films are measured by the space charge-limited current method (SCLC) [45,46]. As shown in Fig. 3c and d, the hole mobility (μ_h) and electron mobility (μ_e) are measured with pure hole devices (PEDOT:PSS/Active Layer/MoO_3/Ag) and pure electron devices (ITO/ZnO/Active Layer/PDINO/Al), respectively. The μ_h and μ_e of the LBL device are 9.94×10^{-4} and 8.48×10^{-4} $cm^2\ V^{-1}\ s^{-2}$ respectively, which are both higher than that of the BHJ device ($\mu_h = 8.12 \times 10^{-4}$ $cm^2\ V^{-1}\ s^{-2}$ and $\mu_e = 5.17 \times 10^{-4}$ $cm^2\ V^{-1}\ s^{-2}$). More importantly, the μ_h/μ_e value of LBL devices (1.17) is closer to 1 than that of BHJ devices (1.57), which indicates that there is a more balanced charge transfer in LBL devices. LBL OSCs exhibit higher charge mobility and more balanced transport compared to BHJ OSCs, which is responsible for the higher J_{SC}, FF, and PCE.

To verify the vertical phase separation of the LBL and BHJ films, the distribution of donor and acceptor on the top surface were investigated by contact angle (CA) measurements [36]. As shown in Fig. 4, CA of PBB-TSD pristine film, Y6 pristine film, LBL and BHJ films were measured with water and diiodomethane (CH_2I_2), and the corresponding surface energy data were calculated by the OWRK method. The surface free energy of PBB-TSD and Y6 pristine film were 39.029 and 44.142 mN m^{-1}, respectively. And the surface free energy of the LBL film (42.093 mN m^{-1}) is closer to Y6 than that of the BHJ film (40.108 mN m^{-1}), which indicates that more Y6 is distributed on the surface and further demonstrates the vertical distribution of D/A within the LBL film. Moreover, the compatibility between the active and interfacial layer films can be quantified by the Flory-Huggins interaction parameter χ. The χ was calculated from the CA results. It's found that χ value is 0.94 between LBL and PDINO film, and 1.44 between BHJ and PDINO film. The low $\chi^{LBL-PDINO}$ indicates a good compatibility between LBL film and PDINO film, which facilitates the reduction of the contact resistance of the two films as discussed above. In addition, good contact between the interface layer and the active layer is conducive to charge transfer and collection, which contributed to the high current of the LBL device in the *J-V* curve.

For OPVs, charge transport are closely related to the morphology of the active layer. As shown in Fig. 5, atomic force microscopy (AFM) and transmission electron microscopy (TEM) were used to study the morphology of the active layer under two different fabrication conditions. The difference in the roughness of the two film surfaces can be found from the height patterns, and the root-mean-square (RMS) value of the LBL films (0.95 nm) is slightly higher than that of the BHJ films (0.73 nm). It can be seen from the TEM plots that the LBL films have larger pure domains of donor and acceptor, which are conducive to the charge transfer. The improved phase aggregation and suitable charge transport paths provide the guarantee of high J_{SC} and PCE of LBL devices. This result confirms that the fabrication method of LBL can adjust

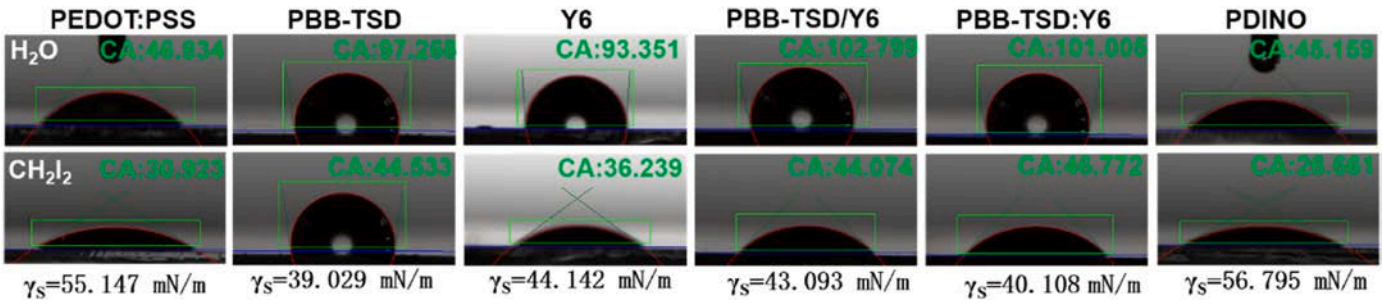

Fig. 4. Contact angles of water or diiodomethane on the PBB-TSD, Y6, LBL and BHJ films.

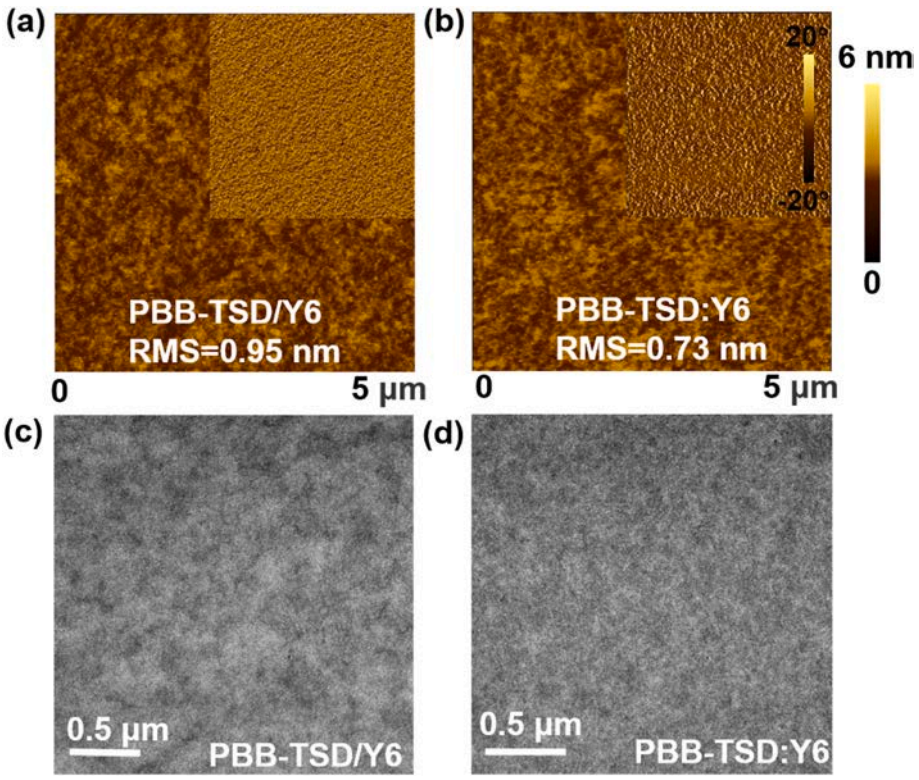

Fig. 5. AFM height and phase (insets) images (top) and TEM images (bottom) of the LBL and BHJ films.

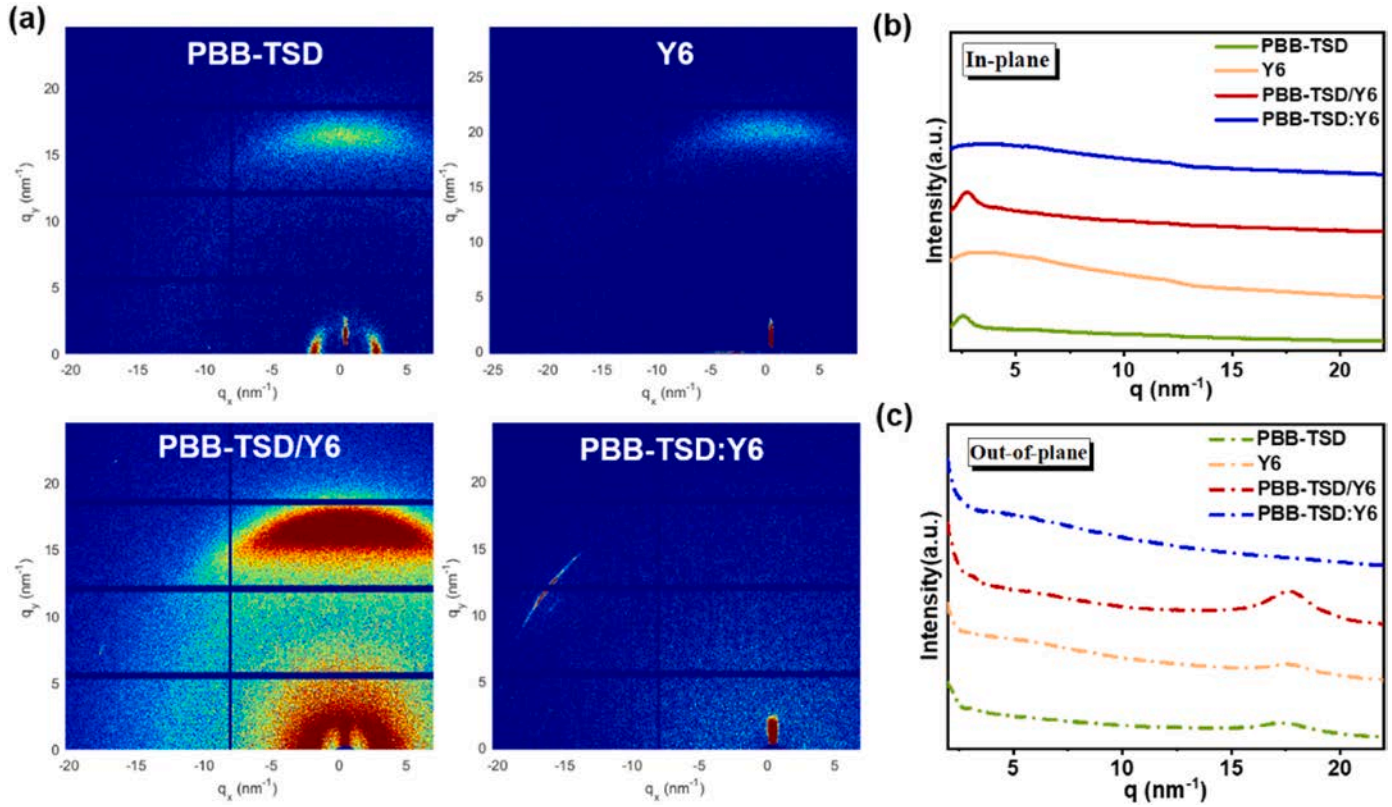

Fig. 6. (a) 2D GIWAXS patterns of pristine PBB-TSD, Y6 and PBB-TSD/Y6 and PBB-TSD:Y6 blend films. Corresponding 1D line-cuts: IP (b) and OOP (c) of the GIWAXS results.

the size of phase domains and aggregation behavior to optimize the morphology, which can facilitate exciton separation and charge transport to achieve higher performance OSCs.

To gain more insight into the structure of LBL and BHJ devices, GIWAXS is used to explore the molecular stacking and crystallization behavior of the thin films [47]. Fig. 6 shows the GIWAXS patterns and associated data of the in-plane (IP) and out-of-plane (OOP) line-cut profiles obtained by Gaussian fitting. PBB-TSD pristine films have distinct π-π stacking (010) diffraction peaks in the OOP direction and (100) lamellar stacking diffraction peaks in the IP direction, indicating that the films are mainly oriented in face-on manner. In addition, the (100) peak extends toward the OOP, indicating the presence of random orientation of the polymer in the film. In the BHJ film, the diffraction peaks are almost invisible in the two-dimensional pattern, which indicate the disorder orientation of PBB-TSD and Y6 in the blend film. The strong diffraction peaks of the LBL films suggest that the PBB-TSD/Y6 film has a favorable face-on orientation, which is a desirable orientation for OSCs to build vertical channels for charge transport. The results could be further proved from the line-cut profiles. Compared with BHJ film, LBL film exhibits enhanced OOP $\pi - \pi$ stacking peak (010) at 17.73 nm^{-1} and enhanced IP lamellar stacking peak (100) at 2.75 nm^{-1}. However, there are no peaks in both OOP and IP orientation of BHJ film. It can be seen that the LBL process results in devices with good crystallinity and face-on orientation, which is beneficial for charge transport and ultimately results in high J_{SC} of LBL devices.

3. Conclusion

In this work, LBL and BHJ OSCs based on PBB-TSD and Y6 are thoroughly investigated. The LBL film shows more ordered molecular stacking and desirable D/A vertical phase separation than that of the BHJ film, which is favorable for reducing charge recombination and promoting charge transport and collection. And the related LBL devices exhibit a more balanced carrier mobility and higher electron and hole mobilities, which realize a high J_{SC} and improved FF. Hence, compared with the BHJ-type OSCs (J_{SC} = 21.19 mA cm^{-2} and FF = 58.05%), the J_{SC} and FF of LBL-type OSCs have been improved to 23.52 mA cm^{-2} and 59.06%, respectively. And the best PCE of 11.84% is obtained in the LBL-type device. Our work shows that the performance of some materials may be not poor, and better device processes need to be developed. The ideal p-i-n like structure for efficient OSCs can be achieved by a simple but effective LBL method, thus facilitating the application of LBL processing methods.

4. Experimental section

Materials. The donor PBB-TSD is synthesized according to our previous works [48,49]. The poly(3,4-ethylenedioxythiophene): poly (styrene sulfonate) (PEDOT: PSS, purchased) is purchased from H.C. Starck co. Ltd., Y6 and PDINO is purchased from Derthon photoelectric material technology Co. Ltd.

Device Fabrication. The OSCs were fabricated based on traditional device structure of ITO/PEDOT: PSS/active layer/PDINO/Al. And the specific fabricating procedure was as follows: Cleaned the ITO-coated glass substrates with deionized water, acetone and isopropyl alcohol by ultrasonic bath sequentially for 15 min in turn. After cleaning, the ITO-coated glass substrates were dried by N_2, and then treated with O_2 plasma for 6 min. PEDOT: PSS was spin coated on ITO-coated glass with 4000 rpm and dried in an oven. For LBL-type OSCs, PBB-TSD and Y6 were dissolved in chloroform at a concentration of 10 and 12 mg/ml, respectively. And the thickness of the LBL film was 140 nm. The two solutions were spin-coated on the PEDOT: PSS film in glove box at 1800 and 2200 rpm successively, followed by 80 °C heating and annealing. For BHJ-type OSCs, the blend solution of PBB-TSD:Y6 was prepared with ratio 1:1.2 in chloroform. The blend solution was spin-coated on the PEDOT: PSS film in glove box at 2500 rpm, followed by 80 °C heating and annealing, and a film with a thickness of 135 nm was obtained. After that, the PDINO solution (1 mg/ml in methanol) was spin-coated on the active layer at 4000 rpm as buffer layer. In the end, an aluminum layer was thermally evaporated below 4×10^{-6} Pa as the cathode. And the effective areas of the solar cells were 0.1 cm^2 as defined by shadow masks.

Device Measurement. The current-density (*J-V*) curves of the OSCs were measured by a Keithley 2420 source meter. The AM 1.5G irradiation was provided by an XES-40S2 (SAN-EI ELECTRIC Co., Ltd) solar simulator (AAA grade, 70 × 70 mm^2 photobeam size) with light intensity of 100 mW cm^{-2}. The absorption spectra of films were measured with a Shimadzu UV-3101 PC spectrometer. The external quantum efficiency (EQE) spectra of OPVs were measured by a Zolix Solar Cell Scan 100. The TEM and TEM images were measured in public laboratory of Qingdao institute of energy. GIWAXS were measured at the synchrotron radiation center of Shanghai light source. Contact angle test: The two liquid method is used to measure the contact angles.

Declaration of competing interest

The authors declare that they have no known competing financial interests or personal relationships that could have appeared to influence the work reported in this paper.

Acknowledgements

This work was supported by the Natural Scientific Foundation of China (51703104), National Key R&D Program of China (2021YFE0190400); the Shandong Provincial Natural Science Foundation (ZR2020MB085, ZR2017BEM035); and the China Postdoctoral Science Foundation (2017M612198). The authors also thank the beamline BL16B1 of Shanghai Synchrotron Radiation Facility for providing the beam time and useful discussion.

References

[1] C. Zhu, L. Meng, J. Zhang, S. Qin, W. Lai, B. Qiu, J. Yuan, Y. Wan, W. Huang, Y. Li, A quinoxaline-based D–A copolymer donor achieving 17.62% efficiency of organic solar cells, Adv. Mater. 33 (2021), 2100474.
[2] W. Yang, W. Wang, Y. Wang, R. Sun, J. Guo, H. Li, M. Shi, J. Guo, Y. Wu, T. Wang, G. Lu, C.J. Brabec, Y. Li, J. Min, Balancing the efficiency, stability, and cost potential for organic solar cells via a new figure of merit, Joule 5 (2021) 1209–1230.
[3] J. Han, F. Bao, D. Huang, X. Wang, C. Yang, R. Yang, X. Jian, J. Wang, X. Bao, J. Chu, A universal method to enhance flexibility and stability of organic solar cells by constructing insulating matrices in active layers, Adv. Funct. Mater. 30 (2020), 2003654.
[4] J. Yuan, Y. Zhang, L. Zhou, G. Zhang, H.-L. Yip, T.-K. Lau, X. Lu, C. Zhu, H. Peng, P. A. Johnson, M. Leclerc, Y. Cao, J. Ulanski, Y. Li, Y. Zou, Single-junction organic solar cell with over 15% efficiency using fused-ring acceptor with electron-deficient core, Joule 3 (2019) 1140–1151.
[5] J. Miao, Y. Wang, J. Liu, L. Wang, Organoboron molecules and polymers for organic solar cell applications, Chem. Soc. Rev. 51 (2022) 153–187.
[6] A.J. Moulé, K. Meerholz, Morphology control in solution-processed bulk-heterojunction solar cell mixtures, Adv. Funct. Mater. 19 (2009) 3028–3036.
[7] F. Zhao, C. Wang, X. Zhan, Morphology control in organic solar cells, Adv. Energy Mater. 8 (2018), 1703147.
[8] Z. Chen, X. Chen, Z. Jia, G. Zhou, J. Xu, Y. Wu, X. Xia, X. Li, X. Zhang, C. Deng, Y. Zhang, X. Lu, W. Liu, C. Zhang, Y. Yang, H. Zhu, Triplet exciton formation for non-radiative voltage loss in high-efficiency nonfullerene organic solar cells, Joule 5 (2021) 1832–1844.
[9] P. Wang, F. Bi, Y. Li, C. Han, N. Zheng, S. Zhang, J. Wang, Y. Wu, X. Bao, Manipulating the intermolecular interactions through side chain engineering and unilateral π-bridge strategy for efficient small molecular photovoltaic acceptor, Adv. Funct. Mater. 32 (2022), 2200166.
[10] M. Ghasemi, N. Balar, Z. Peng, H. Hu, Y. Qin, T. Kim, J.J. Rech, M. Bidwell, W. Mask, I. McCulloch, W. You, A. Amassian, C. Risko, B.T. O'Connor, H. Ade, A molecular interaction–diffusion framework for predicting organic solar cell stability, Nat. Mater. 20 (2021) 525–532.
[11] W. Li, S. Zeiske, O.J. Sandberg, D.B. Riley, P. Meredith, A. Armin, Organic solar cells with near-unity charge generation yield, Energy Environ. Sci. 14 (2021) 6484–6493.
[12] L. Zhan, S. Li, T.-K. Lau, Y. Cui, X. Lu, M. Shi, C.-Z. Li, H. Li, J. Hou, H. Chen, Over 17% efficiency ternary organic solar cells enabled by two non-fullerene acceptors working in an alloy-like model, Energy Environ. Sci. 13 (2020) 635–645.

[13] B. Fan, M. Li, D. Zhang, W. Zhong, L. Ying, Z. Zeng, K. An, Z. Huang, L. Shi, G. C. Bazan, F. Huang, Y. Cao, Tailoring regioisomeric structures of π-conjugated polymers containing monofluorinated π-bridges for highly efficient polymer solar cells, ACS Energy Lett. 5 (2020) 2087–2094.
[14] X. Liu, R. Ma, Y. Wang, S. Du, J. Tong, X. Shi, J. Li, X. Bao, Y. Xia, T. Liu, H. Yan, Significantly boosting efficiency of polymer solar cells by employing a nontoxic halogen-free additive, ACS Appl. Mater. Interfaces 13 (2021) 11117–11124.
[15] Y. Cui, Y. Xu, H. Yao, P. Bi, L. Hong, J. Zhang, Y. Zu, T. Zhang, J. Qin, J. Ren, Z. Chen, C. He, X. Hao, Z. Wei, J. Hou, Single-junction organic photovoltaic cell with 19% efficiency, Adv. Mater. 33 (2021), 2102420.
[16] L. Hong, H. Yao, Y. Cui, P. Bi, T. Zhang, Y. Cheng, Y. Zu, J. Qin, R. Yu, Z. Ge, J. Hou, 18.5% efficiency organic solar cells with a hybrid planar/bulk heterojunction, Adv. Mater. 33 (2021), 2103091.
[17] W. Feng, S. Wu, H. Chen, L. Meng, F. Huang, H. Liang, J. Zhang, Z. Wei, X. Wan, C. Li, Z. Yao, Y. Chen, Tuning morphology of active layer by using a wide bandgap oligomer-like donor enables organic solar cells with over 18% efficiency, Adv. Energy Mater. n/a (2022), 2104060.
[18] C. Han, J. Wang, L. Chen, J. Chen, L. Zhou, P. Wang, W. Shen, N. Zheng, S. Wen, Y. Li, X. Bao, Balancing intermolecular interactions between acceptors and donor/acceptor for efficient organic photovoltaics, Adv. Funct. Mater. 31 (2021), 2107026.
[19] J. Wang, C. Han, F. Bi, D. Huang, Y. Wu, Y. Li, S. Wen, L. Han, C. Yang, X. Bao, J. Chu, Overlapping fasten packing enables efficient dual-donor ternary organic solar cells with super stretchability, Energy Environ. Sci. 14 (2021) 5968–5978.
[20] H. Zhao, B. Lin, J. Xue, H.B. Naveed, C. Zhao, X. Zhou, K. Zhou, H. Wu, Y. Cai, D. Yun, Z. Tang, W. Ma, Kinetics manipulation enables high-performance thick ternary organic solar cells via R2R-compatible slot-die coating, Adv. Mater. 34 (2022), e2105114.
[21] J. Li, N. Wang, Y. Wang, Z. Liang, Y. Peng, C. Yang, X. Bao, Y. Xia, Efficient inverted organic solar cells with a thin natural biomaterial l-arginine as electron transport layer, Sol. Energy 196 (2020) 168–176.
[22] J. Wan, L. Zhang, Q. He, S. Liu, B. Huang, L. Hu, W. Zhou, Y. Chen, High-performance pseudoplanar heterojunction ternary organic solar cells with nonfullerene alloyed acceptor, Adv. Funct. Mater. 30 (2020), 1909760.
[23] C. Yang, C. Zhang, C. Chen, Y. Ren, H. Shen, J. Tong, S. Du, Y. Xia, J. Li, A new alcohol-soluble polymer PFN-ID as cathode interlayer to optimize performance of conventional polymer solar cells by increasing electron mobility, Energy Technol. (2022), 2200199.
[24] C.W. Tang, Two-layer organic photovoltaic cell, Appl. Phys. Lett. 48 (1986) 183–185.
[25] Y. Wang, Y. Wang, L. Zhu, H. Liu, J. Fang, X. Guo, F. Liu, Z. Tang, M. Zhang, Y. Li, A novel wide-bandgap small molecule donor for high efficiency all-small-molecule organic solar cells with small non-radiative energy losses, Energy Environ. Sci. 13 (2020) 1309–1317.
[26] X. Liu, S. Du, Z. Fu, C. Chen, J. Tong, J. Li, N. Zheng, R. Zhang, Y. Xia, Ternary solar cells via ternary polymer donors and third component PC71BM to optimize morphology with 13.15% efficiency, Sol. Energy 222 (2021) 18–26.
[27] W. Feng, S. Wu, H. Chen, L. Meng, F. Huang, H. Liang, J. Zhang, Z. Wei, X. Wan, C. Li, Z. Yao, Y. Chen, Tuning morphology of active layer by using a wide bandgap oligomer-like donor enables organic solar cells with over 18% efficiency, Adv. Energy Mater. (2022), 2104060.
[28] X. Liu, Z. Liang, S. Du, X. Niu, J. Tong, C. Yang, X. Lu, X. Bao, L. Yan, J. Li, Y. Xia, Two compatible acceptors as an alloy model with a halogen-free solvent for efficient ternary polymer solar cells, ACS Appl. Mater. Interfaces 14 (2022) 9386–9397.
[29] Y. Wang, X. Zhan, Layer-by-Layer processed organic solar cells, Adv. Energy Mater. 6 (2016), 1600414.
[30] X. Li, X. Du, J. Zhao, H. Lin, C. Zheng, S. Tao, Layer-by-Layer solution processing method for organic solar cells, Sol. RRL 5 (2020), 2000592.
[31] Y. Lin, L. Ma, Y. Li, Y. Liu, D. Zhu, X. Zhan, Small-Molecule solar cells with fill factors up to 0.75 via a layer-by-layer solution process, Adv. Energy Mater. 4 (2014), 1300626.
[32] H. Chen, T. Zhao, L. Li, P. Tan, H. Lai, Y. Zhu, X. Lai, L. Han, N. Zheng, L. Guo, F. He, 17.6%-Efficient quasiplanar heterojunction organic solar cells from a chlorinated 3D network acceptor, Adv. Mater. 33 (2021), 2102778.
[33] Y. Cui, S. Zhang, N. Liang, J. Kong, C. Yang, H. Yao, L. Ma, J. Hou, Toward efficient polymer solar cells processed by a solution-processed layer-by-layer approach, Adv. Mater. 30 (2018), 1802499.
[34] R. Sun, Q. Wu, J. Guo, T. Wang, Y. Wu, B. Qiu, Z. Luo, W. Yang, Z. Hu, J. Guo, M. Shi, C. Yang, F. Huang, Y. Li, J. Min, A layer-by-layer architecture for printable organic solar cells overcoming the scaling lag of module efficiency, Joule 4 (2020) 407–419.
[35] Q. Wu, W. Wang, Y. Wu, Z. Chen, J. Guo, R. Sun, J. Guo, Y. Yang, J. Min, High-performance all-polymer solar cells with a pseudo-bilayer configuration enabled by a stepwise optimization strategy, Adv. Funct. Mater. 31 (2021), 2010411.
[36] Y. Yan, X. Liu, T. Wang, Conjugated-polymer blends for organic photovoltaics: rational control of vertical stratification for high performance, Adv. Mater. 29 (2017), 1601674.
[37] A. Yi, S. Chae, S. Hong, H.H. Lee, H.J. Kim, Manipulating the crystal structure of a conjugated polymer for efficient sequentially processed organic solar cells, Nanoscale 10 (2018) 21052–21061.
[38] Q. He, W. Sheng, M. Zhang, G. Xu, P. Zhu, H. Zhang, Z. Yao, F. Gao, F. Liu, X. Liao, Y. Chen, Revealing morphology evolution in highly efficient bulk heterojunction and pseudo-planar heterojunction solar cells by additives treatment, Adv. Energy Mater. 11 (2021), 2003390.
[39] R. Sun, J. Guo, C. Sun, T. Wang, Z. Luo, Z. Zhang, X. Jiao, W. Tang, C. Yang, Y. Li, J. Min, A universal layer-by-layer solution-processing approach for efficient non-fullerene organic solar cells, Energy Environ. Sci. 12 (2019) 384–395.
[40] M. Hu, Y. Zhang, X. Liu, X. Zhao, Y. Hu, Z. Yang, C. Yang, Z. Yuan, Y. Chen, Layer-by-Layer solution-processed organic solar cells with perylene diimides as acceptors, ACS Appl. Mater. Interfaces 13 (2021) 29876–29884.
[41] X. Ma, W. Gao, J. Yu, Q. An, M. Zhang, Z. Hu, J. Wang, W. Tang, C. Yang, F. Zhang, Ternary nonfullerene polymer solar cells with efficiency >13.7% by integrating the advantages of the materials and two binary cells, Energy Environ. Sci. 11 (2018) 2134–2141.
[42] Y. Wei, N. Liang, W. Jiang, T. Zhai, Z. Wang, Rylene-fullerene hybrid an emerging electron acceptor for high-performing and photothermal-stable ternary solar cells, Small 18 (2022), 2104060.
[43] V.D. Mihailetchi, H.X. Xie, B. de Boer, L.J.A. Koster, P.W.M. Blom, Charge transport and photocurrent generation in poly(3-hexylthiophene): methanofullerene bulk-heterojunction solar cells, Adv. Funct. Mater. 16 (2006) 699–708.
[44] J. Wang, J. Zhang, Y. Xiao, T. Xiao, R. Zhu, C. Yan, Y. Fu, G. Lu, X. Lu, S.R. Marder, X. Zhan, Effect of isomerization on high-performance nonfullerene electron acceptors, J. Am. Chem. Soc. 140 (2018) 9140–9147.
[45] L. Huang, P. Jiang, Y. Zhang, L. Zhang, Z. Yu, Q. He, W. Zhou, L. Tan, Y. Chen, Unraveling the morphology in solution-processed pseudo-bilayer planar heterojunction organic solar cells, ACS Appl. Mater. Interfaces 11 (2019) 26213–26221.
[46] J. Min, Y.N. Luponosov, N. Gasparini, M. Richter, A.V. Bakirov, M.A. Shcherbina, S. N. Chvalun, L. Grodd, S. Grigorian, T. Ameri, S.A. Ponomarenko, C.J. Brabec, Effects of alkyl terminal chains on morphology, charge generation, transport, and recombination mechanisms in solution-processed small molecule bulk heterojunction solar cells, Adv. Energy Mater. 5 (2015), 1500386.
[47] S. Mukherjee, X. Jiao, H. Ade, Charge creation and recombination in multi-length scale polymer: fullerene BHJ solar cell morphologies, Adv. Energy Mater. 6 (2016), 1600699.
[48] I.O. Raji, S. Wen, Y. Li, D. Huang, X. Shi, A. Saparbaev, C. Gu, C. Yang, X. Bao, Benzobis(Thiazole)-Based conjugated polymer with varying alkylthio side-chain positions for efficient fullerene-free organic solar cells, ACS Appl. Mater. Interfaces 13 (2021) 36071–36079.
[49] S. Wen, Y. Li, N. Zheng, I.O. Raji, C. Yang, X. Bao, High-efficiency organic solar cells enabled by halogenation of polymers based on 2D conjugated benzobis (thiazole), J. Mater. Chem. 8 (2020) 13671–13678.